

Dynamics and bistability in a reduced model of the *lac* operon

Cite as: Chaos **14**, 279 (2004); <https://doi.org/10.1063/1.1689451>

Submitted: 13 March 2003 • Accepted: 04 February 2004 • Published Online: 11 May 2004

Necmettin Yildirim, Moisés Santillán, Daisuke Horike, et al.



View Online



Export Citation

ARTICLES YOU MAY BE INTERESTED IN

[Dynamic behavior in mathematical models of the tryptophan operon](#)

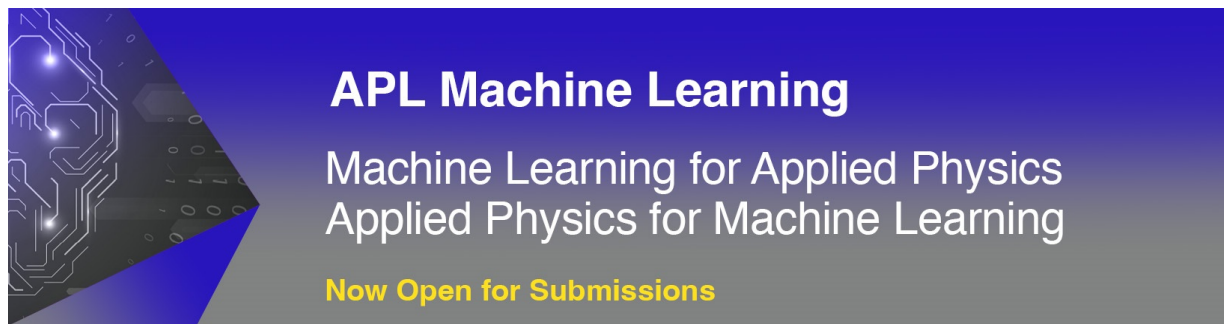
Chaos: An Interdisciplinary Journal of Nonlinear Science **11**, 261 (2001); <https://doi.org/10.1063/1.1336806>

[Bistability in cell signaling: How to make continuous processes discontinuous, and reversible processes irreversible](#)

Chaos: An Interdisciplinary Journal of Nonlinear Science **11**, 227 (2001); <https://doi.org/10.1063/1.1349894>

[Design principles for elementary gene circuits: Elements, methods, and examples](#)

Chaos: An Interdisciplinary Journal of Nonlinear Science **11**, 142 (2001); <https://doi.org/10.1063/1.1349892>



APL Machine Learning

Machine Learning for Applied Physics
Applied Physics for Machine Learning

Now Open for Submissions

Dynamics and bistability in a reduced model of the *lac* operon

Necmettin Yildirim,^{a)} Moisés Santillán,^{b)} and Daisuke Horike^{c)}
Centre for Nonlinear Dynamics, McGill University, Montreal, Quebec H3G 1Y6, Canada

Michael C. Mackey^{d)}
Departments of Physiology, Physics & Mathematics, Centre for Nonlinear Dynamics, McGill University, Montreal, Quebec H3G 1Y6, Canada

(Received 13 March 2003; accepted 4 February 2004; published online 11 May 2004)

It is known that the *lac* operon regulatory pathway is capable of showing bistable behavior. This is an important complex feature, arising from the nonlinearity of the involved mechanisms, which is essential to understand the dynamic behavior of this molecular regulatory system. To find which of the mechanisms involved in the regulation of the *lac* operon is the origin of bistability, we take a previously published model which accounts for the dynamics of mRNA, lactose, allolactose, permease and β -galactosidase involvement and simplify it by ignoring permease dynamics (assuming a constant permease concentration). To test the behavior of the reduced model, three existing sets of data on β -galactosidase levels as a function of time are simulated and we obtain a reasonable agreement between the data and the model predictions. The steady states of the reduced model were numerically and analytically analyzed and it was shown that it may indeed display bistability, depending on the extracellular lactose concentration and growth rate. © 2004 American Institute of Physics. [DOI: 10.1063/1.1689451]

The field of gene regulation has been profoundly influenced by the development of the operon concept. In the 40 years since this notion was put forward, experimentalists have intensively studied regulation in many different systems. However, despite the extensive knowledge of the biology of many of these systems (like the tryptophan and lactose operons) and the wealth of experimental data available about their dynamics, there have been few attempts to integrate this knowledge into coherent mathematical models. In this paper we review previous mathematical treatments of the lactose operon, and then consider a reduced version of the most recent effort by Yildirim and Mackey. By means of a local stability analysis and numerical inspection we show that this reduced model displays bistable behavior. From this, we conclude that of all the *lac* operon regulatory mechanisms, that involving β -galactosidase is directly responsible for bistability in this molecular system. A careful estimation of the parameters in the model allows us to accurately predict experimental data from three different experimental situations in which the temporal evolution of a critical component of the lactose operon was monitored following a perturbation. This last result supports the conclusion that

the β -galactosidase regulatory pathway is, perhaps, the most essential of the regulatory mechanisms in the *lac* operon.

I. INTRODUCTION

It is almost universally accepted that the concept of operon,¹ introduced by Jacob *et al.*,² has had a profound and probably lasting effect on the face of the biological and medical sciences that is still unfolding. The most extensively studied operons are the tryptophan and the lactose operons, which have been acknowledged as the paradigms of repressible and inducible operons, respectively. Although not recognized as such at the time, the lactose operon was one of the first molecular systems experimentally demonstrated to display bistable behavior.³ Among the various patterns of behavior emerging from regulation associated with nonlinear kinetics, bistability is extremely interesting. Bistability allows a true discontinuous switching (with hysteresis) between alternate steady states that can convert graded inputs into switch-like responses. This permits a discontinuous evolution of the system along different possible pathways, which can be either reversible or irreversible, and may provide the system with an epigenetic (nongenetic, hereditary) memory. The evolutionary significance of bistability, as well as its possible role in explaining some basic processes of life, like cell differentiation or the maintenance of phenotypic differences in the absence of genetic and environmental differences, has recently been discussed elsewhere.^{4–6}

A number of mathematical models of the lactose operon have been developed with different goals.^{4,7–20} However, to our knowledge, only two of these^{4,20} deal with the issue of bistability in the lactose operon. Laurent and Kellersohn⁴ introduced a simple model of the lactose operon that, with a

^{a)}Permanent address: Atatürk Üniversitesi, Bilgisayar Bilimleri Uygulama ve Araştırma Merkezi, 25240 Erzurum, Turkey.

^{b)}Permanent address: Depto. de Física, Esc. Sup. de Física y Matemáticas, Instituto Politécnico Nacional, Edif. 9, U. P. Zacatenco, 07738 México D. F., México.

^{c)}Permanent address: Department of Mathematical Sciences, Graduate School of Science and Engineering, Waseda University, Japan.

^{d)}Author to whom correspondence should be addressed. 3655 Promenade Sir William Osler, Room 1124, Montreal, Quebec H3G 1Y6, Canada. Telephone: (514) 398-4336; fax: (514) 398-7452. Electronic mail: mackey@cnd.mcgill.ca

proper choice of the parameter values, was able to show bistable behavior. More recently, Yildirim and Mackey²⁰ developed a more detailed mathematical model in which the parameters were all estimated from reported experimental data, and showed that, indeed, there is bistability in the lactose operon dynamics for realistic extracellular lactose concentration values.

The model of Yildirim and Mackey includes the time delays due to transcription and translation, as well as most of the lactose operon regulatory mechanisms. It considers neither inducer exclusion nor catabolite repression (two external-glucose dependent mechanisms). Despite this omission, the Yildirim and Mackey model is capable of displaying bistability, indicating that bistability does not rely on the presence of glucose in the extracellular medium. These results suggest two different pathways for future research: To investigate the influence of the glucose dependent mechanisms on the bistable behavior of the lactose operon, and to find out whether there exists a subset of the mechanisms considered in the Yildirim and Mackey capable of accounting for bistability.

Of the three genes comprised by the lactose operon, only two encode for proteins involved in its regulation. These proteins are β -galactosidase and lactose permease and the two of them participate in positive feedback loops capable, in principle, of generating bistability. In the present work a simplification of the Yildirim and Mackey model, that considers only the role of β -galactosidase in the operon regulation and ignores that of lactose permease, is introduced. By numerically solving the time-delay differential equations of the reduced model and by performing a local stability analysis we show that it reproduces dynamic experimental data as well as the complete model and that it displays bistability. From this, we conclude that of all the lactose operon regulatory mechanisms, that involving β -galactosidase is the one directly responsible for bistability in this molecular system.

The outline of the paper is as follows. In Sec. II we describe the Yildirim–Mackey model for the *lac* operon. In Sec. III we consider a reduced version of this model that allows more detailed mathematical analysis, and summarize the results of our parameter estimation that are detailed in Appendix A. Then in Sec. IV we examine the steady states of the system and show that depending on the growth rate and lactose levels there may be one, two, or three steady states. We have determined the ranges over which these steady states may exist based on our parameter estimation, and also shown that when a single steady state exists it is stable while when three of them exist, two are locally stable and the intermediate one is unstable. In Sec. V we have used the reduced model to predict the response to three different experimental conditions and compared the model response to previously published experimental data, finding good agreement. The paper concludes with Sec. VI in which we summarize our findings, and briefly discuss other operon modeling efforts.

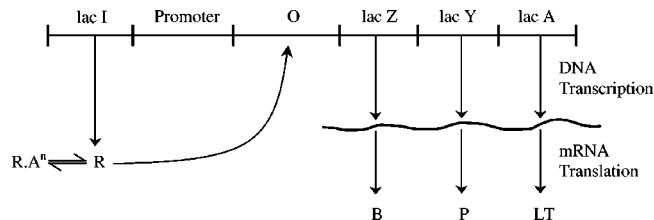


FIG. 1. A diagrammatic representation of the *lac* operon. *R* is the *lac* repressor produced by the regulatory operon *lacI*, *O* the operator region, and *lacZ*, *lacY*, and *lacA* are the three structural genes that make up the operon. *B* stands for β galactosidase, *P* for permease, *A* for allolactose, and *LT* for thiogalactoside transacetylase.

II. THE YILDIRIM AND MACKEY MODEL

In describing the Yildirim and Mackey model²⁰ for regulation of the *lac* operon, we must first consider the dynamics of mRNA induction. To this end, it will be helpful in the following discussion to refer to Fig. 1.

The *lac* operon consists of a small promoter–operator region and three larger structural genes *lacZ*, *lacY*, and *lacA*. Preceding the *lac* operon is a regulatory operon *lacI* denoted by (*R*) that is responsible for producing a repressor (*R*) protein. In the absence of allolactose (*A*) the repressor *R* binds to the operator region *O* and prevents the RNA polymerase (which binds to the promoter region) from transcribing the structural genes. However, in the presence of allolactose, a complex is formed between allolactose and the repressor that makes binding of the repressor to the operator region impossible. In that case, the RNA polymerase bound to the promoter is able to initiate transcription of the structural genes to produce mRNA.

Once the production of mRNA has been started through DNA transcription, the process of translation is initiated. The *lacZ* gene encodes the portion of the mRNA that is responsible for the production of β -galactosidase (*B*) and transcription of the *lacY* gene produces the section of mRNA ultimately responsible for the production of a permease (*P*). The final portion mRNA produced by transcription of the *lacA* gene encodes for the production of thiogalactoside transacetylase which is thought to not play a role in the regulation of the *lac* operon²¹ and which will not be further considered here.

In words, the way this control system works is the following (cf. Fig. 2). In the absence of glucose available for cellular metabolism, but in the presence of lactose (*L*), lactose is transported into the cell by the permease. This intracellular lactose is then broken down into glucose, galactose, and allolactose by β -galactosidase. The allolactose is also converted to glucose and galactose by β -galactosidase. The allolactose feeds back to bind with the lactose repressor and enable the transcription process.

Let *R* be the repressor and *O* the operator. The effector allolactose binds with the active form *R* of the repressor and Yagil and Yagil²² have shown that data on the fraction *F* of free operator sites as a function of allolactose levels can be accurately fit by

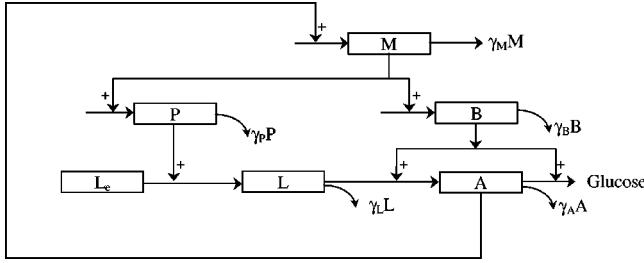


FIG. 2. A diagrammatic representation of the *lac* operon feedback control loop. M is the mRNA concentration, B the β galactosidase concentration, A the concentration of allolactose, L is the intracellular lactose concentration, L_e the external lactose concentration, and P is the concentration of permease. Although we have indicated that only allolactose is converted to glucose (and galactose) by β -galactosidase, there is also a conversion pathway from lactose to glucose and galactose that is not indicated but which is accounted for in the full model. For every species i , the parameter γ_i indicates the corresponding degradation rate.

$$F(A) = \frac{1 + K_1 A^n}{K + K_1 A^n}, \quad (1)$$

where n , K , and K_1 are positive constants. There will be maximal repression when $A=0$ but that at this point there will still be a basal level of mRNA production proportional to K^{-1} .

Having a relation between the fraction of operators free to synthesize mRNA and the level of the effector A , we are now in a position to describe the model for *lac* operon regulation. In what follows, continued reference to Fig. 2 will be useful. We let M be the mRNA concentration, B the β galactosidase concentration, A the concentration of allolactose (the effector in the *lac* operon), L the lactose concentration, L_e the external lactose concentration, and P the concentration of permease. The bacterial growth rate is given by μ .

The dynamics of mRNA production are given in Eq. (2),

$$\frac{dM}{dt} = \alpha_M \frac{1 + K_1 (e^{-\mu \tau_M} A_{\tau_M})^n}{K + K_1 (e^{-\mu \tau_M} A_{\tau_M})^n} - \tilde{\gamma}_M M, \quad (2)$$

$$A_{\tau_M} \equiv A(t - \tau_M),$$

and can be understood as follows. First we note that the production of mRNA from DNA via transcription is not an instantaneous process but in fact requires a period of time τ_M for RNA polymerase to transcribe the first ribosome binding site. The rate of change of M is made up of a balance between a production term $\alpha_M F$ and a loss term $\tilde{\gamma}_M M$. The argument of F in the production term is $e^{-\mu \tau_M} A_{\tau_M}$ where $A_{\tau_M} \equiv A(t - \tau_M)$. The exponential prefactor $e^{-\mu \tau_M}$ accounts for the dilution of the allolactose through growth during the transcriptional period.²³ The loss term in Eq. (2), $\tilde{\gamma}_M M \equiv (\gamma_M + \mu)M$, is made up of an mRNA degradation term, $\gamma_M M$, and an effective loss due to dilution, μM .

Turning now to the dynamics of β -galactosidase as captured in Eq. (3),

$$\frac{dB}{dt} = \alpha_B e^{-\mu \tau_B} M_{\tau_B} - \tilde{\gamma}_B B, \quad M_{\tau_B} \equiv M(t - \tau_B), \quad (3)$$

we observe that the production of β -galactosidase through translation of the mRNA is also not an instantaneous process but requires a time τ_B . Then we simply assume that the rate of production of B is directly proportional to the concentration of M a time τ_B ago ($\alpha_B e^{-\mu \tau_B} M_{\tau_B}$), where again the exponential factor takes into account the dilution of mRNA due to cell growth. The rate of loss of B is given by $\tilde{\gamma}_B B$, where as before $\tilde{\gamma}_B = (\gamma_B + \mu)$.

For lactose, things become somewhat more complicated since the dynamics are given by

$$\frac{dL}{dt} = \alpha_L P \frac{L_e}{K_{L_e} + L_e} - \beta_{L_1} P \frac{L}{K_{L_1} + L} - \beta_{L_2} B \frac{L}{K_{L_2} + L} - \tilde{\gamma}_L L. \quad (4)$$

The first term on the right-hand side of Eq. (4) has to do with gain of intracellular lactose L because of the permease facilitated transport of L_e , and the proportionality constant α_L is a decreasing function of extracellular glucose.²⁴ The second term expresses the loss of intracellular lactose to the extracellular fluid due to the reversible nature of the permease mediated transport.^{24–27} The coefficient β_{L_1} is not dependent on the external glucose levels. The third term accounts for the β -galactosidase (B) mediated conversion of lactose to allolactose as well as the hydrolysis of lactose to glucose and galactose (not indicated in Fig. 2), while the fourth and final term again accounts for the decrease in internal lactose concentration due to degradation and dilution ($\tilde{\gamma}_L = \gamma_L + \mu$).

For the allolactose dynamics we have

$$\frac{dA}{dt} = \alpha_A B \frac{L}{K_L + L} - \beta_A B \frac{A}{K_A + A} - \tilde{\gamma}_A A. \quad (5)$$

The first term on the right-hand side of Eq. (5) gives the gain in allolactose due to the conversion of lactose mediated by β -galactosidase. The second term denotes the loss of allolactose due to its conversion to glucose and galactose (again mediated by β -galactosidase), and the last term accounts for the degradation and dilution of allolactose.

Finally, to describe the permease dynamics we have

$$\frac{dP}{dt} = \alpha_P e^{-\mu \tau_P} M_{\tau_P} - \tilde{\gamma}_P P. \quad (6)$$

In Eq. (6) the first term reflects the assumption that the permease production is directly proportional (proportionality constant α_P) to the mRNA concentration a time (τ_P) in the past, where τ_P is the translation time between mRNA and permease. The exponential prefactor again accounts for dilution of mRNA concentration due to cell growth. The second term merely accounts for the degradation and dilution of permease.

The regulatory aspects of this control system are numerous, the most prominent being the nonlinear dependence of the fraction of free operator sites on the allolactose levels in Eq. (2). However, the nonlinearities in Eqs. (4) and (5) also play a role.

TABLE I. The estimated parameters for the reduced model. See Appendix A for the details of their determination.

Parameter	Value
μ_{\max}	$3.47 \times 10^{-2} \text{ min}^{-1}$
$\bar{\mu}$	$3.03 \times 10^{-2} \text{ min}^{-1}$
α_M	$997 \text{ nM} \cdot \text{min}^{-1}$
α_B	$1.66 \times 10^{-2} \text{ min}^{-1}$
α_A	$1.76 \times 10^4 \text{ min}^{-1}$
γ_M	0.411 min^{-1}
γ_B	$8.33 \times 10^{-4} \text{ min}^{-1}$
γ_A	$1.35 \times 10^{-2} \text{ min}^{-1}$
n	2
K	7200
K_1	$2.52 \times 10^{-2} (\mu\text{M})^{-2}$
K_L	0.97 mM
K_A	1.95 mM
β_A	$2.15 \times 10^4 \text{ min}^{-1}$
τ_M	0.10 min
τ_B	2.00 min

III. A REDUCED MODEL

The full model of the previous section, consisting of Eqs. (2)–(6), has been studied numerically by Yildirim and Mackey,²⁰ but is too complicated for a complete analysis. Moreover, we are interested in determining whether the β -galactosidase regulatory pathway can account for the *lac* operon bistable behavior by itself. Thus we have reduced the complexity of the model through a single assumption. We assume that there is a constant permease concentration, that lactose is in a quasisteady state across the membrane, and that, therefore, there is a one-to-one relationship between the external and internal lactose. With these assumptions we can take internal lactose to be a parameter and eliminate Eq. (4) from the model.²⁸ Since we do not consider lactose dynamics there is no need to deal with the permease dynamics as embodied in Eq. (6). The consequence of these assumptions is that our system of five differential delay equations can be reduced to a three dimensional system:

$$\frac{dM}{dt} = \alpha_M \frac{1 + K_1(e^{-\mu\tau_M A})^n}{K + K_1(e^{-\mu\tau_M A})^n} - \tilde{\gamma}_M M, \quad (7)$$

$$\frac{dB}{dt} = \alpha_B e^{-\mu\tau_B M} - \tilde{\gamma}_B B, \quad (8)$$

and

$$\frac{dA}{dt} = \alpha_A B \frac{L}{K_L + L} - \beta_A B \frac{A}{K_A + A} - \tilde{\gamma}_A A. \quad (9)$$

We have estimated the parameters for the reduced model in Appendix A, and the results of that procedure are summarized in Table I. The growth rate μ of *E. coli* can be highly variable and ranges between 0 and a maximal value of $\mu_{\max} = 3.47 \times 10^{-2} \text{ min}^{-1}$. To study our model numerically and test its predictions against experimental data we have estimated a single growth rate $\bar{\mu}$ from the data of Knorre.²⁹ This estimation, which is detailed in Appendix A, yielded $\bar{\mu} = 3.03 \times 10^{-2} \text{ min}^{-1}$ which is the value we have consistently used throughout for our numerical computations.

IV. STEADY STATES AND THEIR STABILITY

Scaling the variables in Eqs. (7)–(9) to a dimensionless form by defining new variables

$$\tau = \tau_M + \tau_B, \quad a = \sqrt[n]{K_1} A,$$

$$\hat{t} = \frac{t}{\tau}, \quad b = \sqrt[n]{K_1} B,$$

$$\hat{\tau}_M = \frac{\tau_M}{\tau}, \quad m = \sqrt[n]{K_1} M,$$

$$\hat{\tau}_B = \frac{\tau_B}{\tau}, \quad l = \sqrt[n]{K_1} L,$$

$$\hat{\mu} = \mu \tau,$$

allows us to write Eqs. (7)–(9) in the dimensionless representation

$$\frac{dm}{d\hat{t}} = \hat{\alpha}_M f(a_{\hat{\tau}_M}) - \hat{\gamma}_M m, \quad (10)$$

$$\frac{db}{d\hat{t}} = \hat{\alpha}_B e^{-\hat{\mu} \hat{\tau}_B m \hat{\tau}_B} - \hat{\gamma}_B b, \quad (11)$$

and

$$\frac{da}{d\hat{t}} = \hat{\alpha}_A h(l)b - \hat{\beta}_A g(a)b - \hat{\gamma}_A a. \quad (12)$$

In this representation,

$$f(a_{\hat{\tau}_M}) = \frac{1 + \varpi a_{\hat{\tau}_M}^n}{K + \varpi a_{\hat{\tau}_M}^n}, \quad \text{where } \varpi = e^{-n\hat{\mu}\hat{\tau}_M}, \quad (13)$$

$$h(l) = \frac{l}{\sqrt[n]{K_1} K_L + l}, \quad (14)$$

and

$$g(a) = \frac{a}{\kappa + a}, \quad (15)$$

and the dimensionless parameters are defined by

$$\hat{\alpha}_M = \tau^n \sqrt[n]{K_1} \alpha_M, \quad \hat{\gamma}_M = \tau \tilde{\gamma}_M, \quad \hat{\alpha}_B = \tau \alpha_B,$$

$$\hat{\gamma}_B = \tau \tilde{\gamma}_B, \quad \kappa = \sqrt[n]{K_1} K_A, \quad \hat{\alpha}_A = \tau \alpha_A,$$

$$\hat{\gamma}_A = \tau \tilde{\gamma}_A, \quad \hat{\beta}_A = \tau \beta_A.$$

Let (m_*, a_*, b_*) be a steady state of the system. From Eqs. (10) and (12), we have

$$m_* = \frac{\hat{\alpha}_M}{\hat{\gamma}_M} f(a_*) \quad (16)$$

and

$$b_* = \frac{\hat{\gamma}_A a_*}{\hat{\alpha}_A h(l) - \hat{\beta}_A g(a_*)}. \quad (17)$$

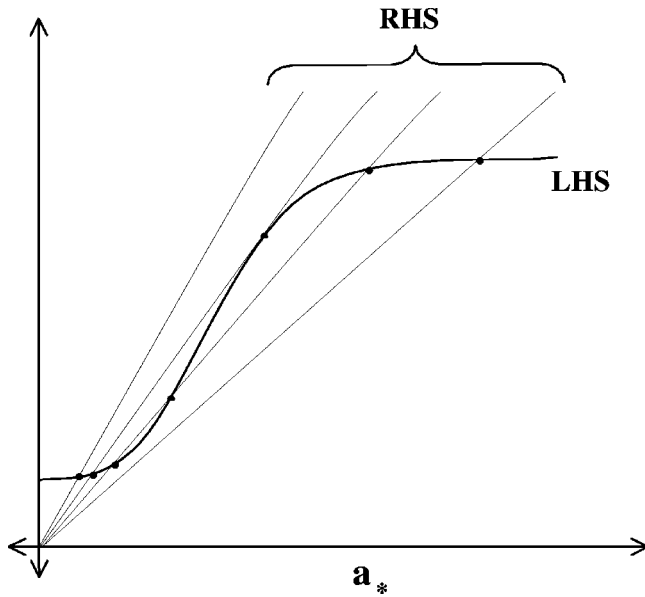


FIG. 3. A diagrammatic representation showing how one, two or three steady states may arise in the simplified *lac* operon model whose steady states are defined by Eq. (19). The right (left) hand sides of Eq. (19) are denoted by RHS (LHS), and the intersection of the two curves gives the location of a steady state.

For a biologically meaningful (non-negative) steady state value of b_* , the denominator of Eq. (17) must be non-negative. Further, from Eq. (11)

$$m_* = \frac{\hat{\gamma}_B e^{\hat{\mu} \hat{\tau}_B}}{\hat{\alpha}_B} b_* . \quad (18)$$

Substituting Eqs. (16) and (17) into Eq. (18), we obtain the equation

$$f(a_*) = \Theta \frac{a_*}{h(l) - \frac{\hat{\beta}_A}{\hat{\alpha}_A} g(a_*)} , \quad (19)$$

defining the steady states results, where the constant Θ is given by

$$\Theta = \frac{\hat{\gamma}_A \hat{\gamma}_B \hat{\gamma}_M e^{\hat{\mu} \hat{\tau}_B}}{\hat{\alpha}_B \hat{\alpha}_M \hat{\alpha}_A} . \quad (20)$$

An examination of Eq. (19) when $K > 1$ reveals that the left hand side is a monotone increasing function of a_* with a minimal value of $f(0) = 1/K$ at $a_* = 0$ and a maximal value of 1 for large values of the steady state allolactose levels. The right hand side is also a monotone increasing function of a_* that is zero at $a_* = 0$. A simple graphical argument shows that with $n = 2$ as we have estimated there may be one, two, or three steady states depending on the values of the growth rate μ or lactose concentration L as shown in Fig. 3. We denote these dimensionless steady states by a_*^i , $i = 1, 2, 3$, wherein $0 < a_*^1 \leq a_*^2 \leq a_*^3$. (The corresponding actual steady states are denoted by A_*^i , $i = 1, 2, 3$.) Analytical conditions for the existence of these steady states are given in Appendix

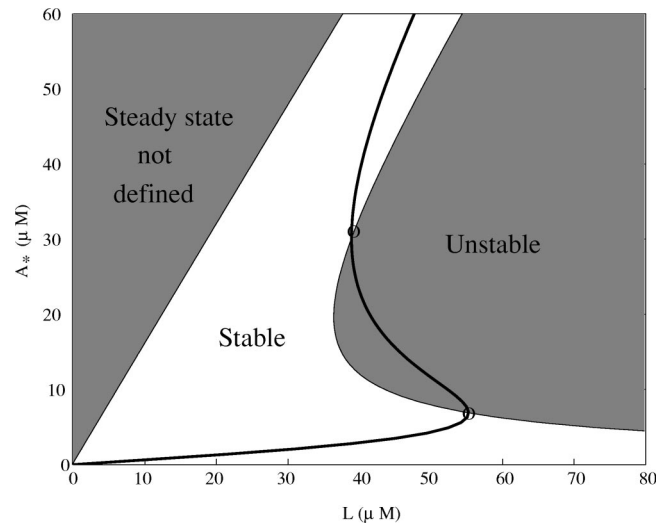


FIG. 4. Numerical depiction of the stable and unstable regions of the lactose-allolactose space and the steady states as a function of lactose levels for the reduced model when all parameters are held at their estimated values in Table I when $\bar{\mu} = 3.03 \times 10^{-2} \text{ min}^{-1}$. For a given value of lactose concentration L , the corresponding allolactose-concentration steady state values (A_*) are determined by the intersection of the solid-line curve and a vertical $L = \text{constant}$ straight line (not shown). The stability properties of a given steady state depend on the region it falls in. The lactose level corresponding to the right most point marked by the “o” corresponds to the minimum level required for induction of the *lac* operon, and our numerical computations predict this value to be $55.43 \mu\text{M}$. The analysis of Appendix C shows that if the delays are neglected (set identically to zero), then the induction point is shifted to $52.10 \mu\text{M}$.

B. For the parameter values given in Table I, the range of internal lactose concentrations over which three steady states exist is computed to be $(39.10, 55.43) \mu\text{M}$.

In Appendix C we have determined the linear stability of the steady states of this model. The results of that relatively tedious analysis show that the steady states a_*^1 and a_*^3 are always locally stable and the steady state a_*^2 is always unstable. This is illustrated in Fig. 4. In Appendix D, we examine the intersection points between the steady state curve $A_*(L)$ and the stability boundary when there is the possibility of three coexisting steady states.

An examination of the dependence of the criteria for the existence of steady states a_* (or A_*) on (μ, L) in Appendix E reveals that the number of steady states depend on the growth rate μ and lactose level L . According to our computations, the system can only show bistable behavior for growth rates equal to or larger than $\mu_0 = 1.52 \times 10^{-2} \text{ min}^{-1}$ which corresponds to a doubling time of $(\ln 2)/(1.52 \times 10^{-2}) \text{ min} = 45.6 \text{ min}$. This bifurcation in the model in (μ, L) space or plane is depicted in Fig. 5. As illustrated in the figure, for values of the growth rate $\mu \in [0, \mu_0)$ there is a unique steady state level of allolactose A_* for any given value of lactose levels L . However, as μ becomes larger, $\mu \in [\mu_0, \mu_{\max}]$, the system may have multiple steady states values of A_* at a given lactose level L . (See Appendix E for details of determination of the value of μ_0 demarcating the boundary between single and multiple steady states.) The interesting aspect of this bifurcation and the attendant predicted bistability of allolactose and mRNA levels is that it

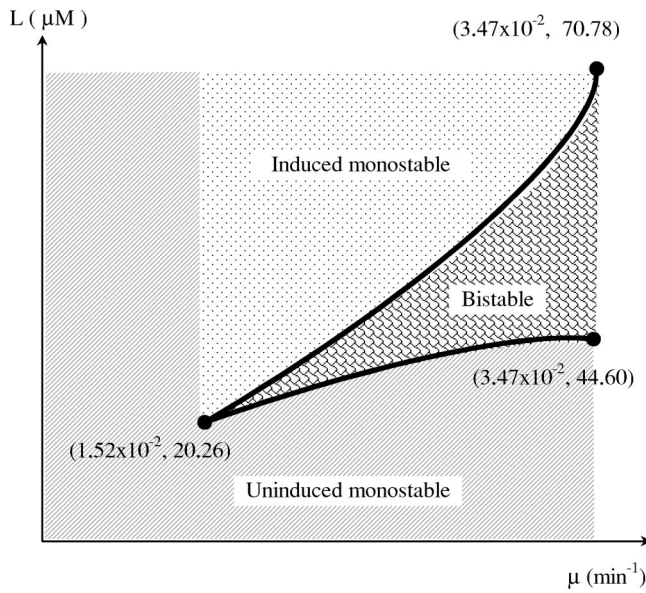


FIG. 5. Bifurcations in (μ, L) space for the reduced model when all parameters except μ are held at their estimated values listed in Table I. As detailed in Appendix E, for values of $\mu < \mu_0 \approx 1.52 \times 10^{-2} \text{ min}^{-1}$ there is a single steady state, and for $\mu \in (\mu_0, \mu_{\max})$, where $\mu_{\max} \approx 3.47 \times 10^{-2} \text{ min}^{-1}$, there are two co-existing locally stable steady states.

should be possible to demonstrate experimentally if our model has any biological validity.

V. NUMERICAL SIMULATIONS

The analytical results of the stability analysis of the reduced model given in Appendix C were tested by numerically integrating the system of three differential delay equations, and the results are reported in this section. We used MATLAB'S DDE23 routine³⁰ for the numerical solution of the delayed system with $L = 50 \text{ } \mu\text{M}$ for the internal lactose concentration. At this value, the system has the following three steady states:

$$\text{SS1:}(A_*, B_*, M_*) = (4.27 \text{ } \mu\text{M}, 0.23 \text{ nM}, 0.46 \text{ nM}),$$

$$\text{SS2:}(A_*, B_*, M_*) = (11.73 \text{ } \mu\text{M}, 0.70 \text{ nM}, 1.39 \text{ nM}),$$

$$\text{SS3:}(A_*, B_*, M_*) \\ = (64.68 \text{ } \mu\text{M}, 16.42 \text{ nM}, 32.71 \text{ nM}).$$

We found numerically that the system converged to the steady state values corresponding to either the lower or upper branches of the S-shaped curve in Fig. 4 for various initial values. For the simulations shown in Fig. 6, the concentration units are in nM and time is in minutes. The initial values of both allolactose and mRNA concentrations were kept constant at their steady state values on the lower branch of the S-shaped curve when $L = 50 \text{ } \mu\text{M}$, and six initial values of the β -galactosidase concentration were taken equally spaced between 0.6 and 1.6 nM.

For initial values of the β -galactosidase concentration less than 1.2 nM, the β galactosidase levels converged to 0.23 nM which is the steady state value of β galactosidase corresponding to the lower branch of S-shaped curve in Fig. 4. However, for the three initial values of β galactosidase

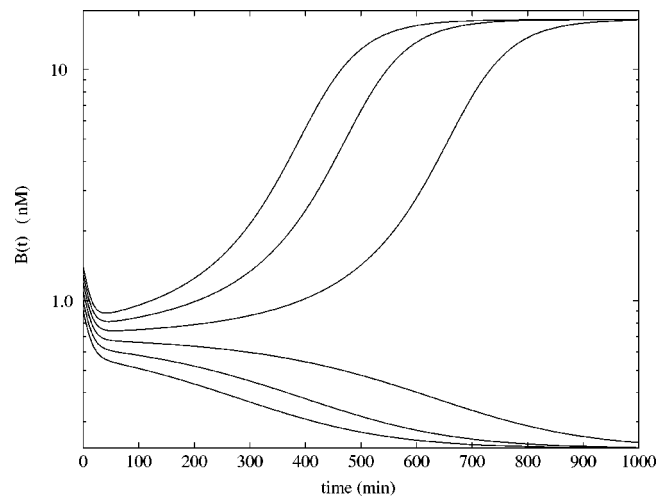


FIG. 6. Bistability arising in the numerical simulation of β -galactosidase concentration versus time (min) with the parameters of Table I, except $\bar{\mu} = 3.03 \times 10^{-2} \text{ min}^{-1}$, for various starting values of β -galactosidase when $L = 50 \text{ } \mu\text{M}$, which is in the range of lactose concentration for existence of three steady states. The selection of the six initial conditions is described in the text. Note that the β -galactosidase scale is logarithmic.

equal to or greater than 1.2 nM, the β galactosidase concentration converged to 16.42 nM, which is the steady state value of β galactosidase on the upper branch of the curve in Fig. 4. These plus other simulations (not shown) suggest that the local stability results of Appendix C apply over a wide range of initial conditions.

We have studied the reduced model both analytically and numerically and found that it is capable of displaying bistability for a realistic range of μ and L values. These results are in agreement with those obtained by Yildirim and Mackey²⁰ with a more detailed model. To further test the accuracy of the reduced model we studied the ability of our model to predict three different experimental data sets taken from the published literature. The first data set is from Knorre.²⁹ In that paper, changes of the specific β galactosidase activity after a step change from glucose to lactose growth for *E. coli* ML 30 were measured experimentally. The second data set, from Pestka et al.,³¹ was obtained in a study of the specific inhibition of translation of single mRNA molecules and gave the specific activity of β galactosidase versus time for *E. coli* 294 in the presence of IPTG. These two sets of data and the simulated curve produced by the model using MATLAB'S DDE23 routine³⁰ are shown in Fig. 7. The initial conditions were taken as the steady state values when $L = 50 \text{ } \mu\text{M}$ on the lower branch. The curve was produced running the simulation for the lactose value of $L = 600 \text{ } \mu\text{M}$ which corresponds a steady state value on the upper branch of the S-shaped curve. As seen from Fig. 7, there is relatively good agreement between the experimental data and the model predicted curve for β galactosidase concentration. (Note that in this and the next figure, we have scaled the data since there is no correspondence available between β galactosidase concentration and activity.)

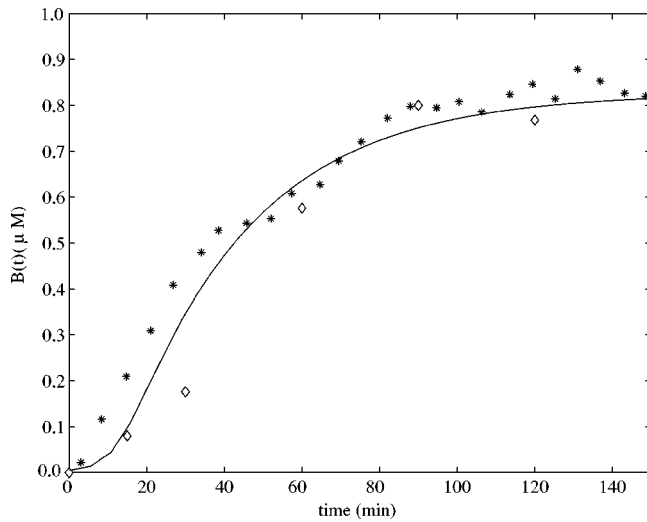


FIG. 7. β -galactosidase concentration vs time. The experimental data sets taken from Knorre (Ref. 29) for *E. coli* ML30 (*) and from Petska *et al.* (Ref. 31) for *E. coli* 294 (◇) as well as the model simulation (solid line) using the parameters of Table I, with $\bar{\mu} = 3.03 \times 10^{-2} \text{ min}^{-1}$, are both shown. The selection of initial conditions and internal lactose concentration are described in the text.

As a third test, a data set from Goodwin³² was used. In this paper, the dynamic behavior of β galactosidase was studied in chemostat cultures of *E. coli* synchronized with respect to cell division by periodic phosphate feeding at a period T equal to the bacterial doubling time. Stable oscillations in β galactosidase concentration were observed with a period equal to the feeding period.

To imitate periodic phosphate feeding in our simulation, we assumed that the bacterial growth rate varies as a function of time in the form given by

$$\mu(t) = \bar{\mu} - \alpha \text{ mod}(t, T). \quad (21)$$

Here, T is the period of the feeding and α is a positive parameter with dimension min^{-2} . $\text{mod}(t, T)$ is a function that gives the remainder on division of t by T . Selection of this type of function is motivated by the observation that growth rates decrease as nutrient levels fall and sharply increase upon the addition of nutrient. $\mu(t)$ is a bounded and positive definite function and takes its maximal value of $\bar{\mu}$ when time is $t = T \times k$, ($k = 1, 2, 3, \dots$) which corresponds to the times that phosphate was added.

If $y(t)$ is the population density, then between one feeding and the next the population numbers are governed by

$$\frac{1}{y} \frac{dy}{dt} = \bar{\mu} - \alpha t,$$

so $\ln 2 = \bar{\mu}T - \alpha T^2/2$ under the assumption that T is also the doubling time. From this we have immediately that

$$\alpha = \frac{2\bar{\mu}}{T} - \frac{2 \ln 2}{T^2}.$$

With a feeding period of $T = 100$ minutes and $\bar{\mu} = 3.03 \times 10^{-2} \text{ min}^{-1}$, $\alpha \approx 4.67 \times 10^{-4} \text{ min}^{-2}$. In Fig. 8, we compare the data on β galactosidase activity during periodic feeding as a function of time with the model predictions.

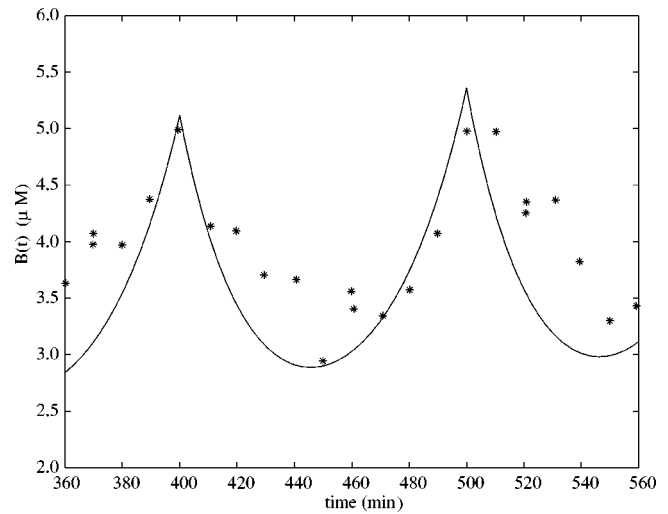


FIG. 8. Oscillation in β -galactosidase concentration in response to periodic phosphate feeding with period $T = 100$ minutes, which is equal to the culture doubling time. The experimental data (*) together with the model simulation (solid line) using the parameters of Table I with a growth rate $\mu(t)$ given by Eq. (21) and $\bar{\mu} = 3.03 \times 10^{-2} \text{ min}^{-1}$ are presented. The experimental data are taken from Goodwin (Ref. 32). The simulation was calculated by numerically solving the system of delay differential equations given by Eqs. (7)–(9). The initial conditions were taken to be the steady state values on the upper branch of S shape curve when $L = 600 \text{ } \mu\text{M}$.

VI. CONCLUSIONS AND DISCUSSION

Yildirim and Mackey²⁰ recently published a model of the lactose operon in which the independent variables are permease, β -galactosidase and lactose concentrations and considers bacterial growth, positive feedback regulation of mRNA production by allolactose, positive feedback lactose intake by permease, and the time delays due to DNA transcription and mRNA translation. In this model, the total operator and repressor concentrations are assumed constant and it is assumed that the amount of repressor bound to the operator region is small compared to the total repressor concentration. Other features were ignored (such as negative feedback due to catabolite repression).

In this paper, we simplified the Yildirim and Mackey model by ignoring the positive feedback loop involving permease, and therefore, assuming equilibration of intra- and extra-cellular lactose. The rationale for this simplification is to figure out whether the positive feedback regulation of mRNA production by allolactose is sufficient to account for important dynamic features of the lactose operon, like bistability. The reduced model consists of a system of three differential delay equations with two delays. Special attention was given to the estimation of the system parameters from data in the literature. The results are clear. Namely, this regulatory pathway is sufficient to account for bistability at physiologically realistic extracellular lactose values. Furthermore, the predicted bistability occurs for lactose values not significantly different from those of the full Yildirim and Mackey model.

The steady states of the reduced model were analyzed both numerically and analytically. We have shown that the model can display bistability for realistic range values of the bacterial growth rate as well as the internal lactose concen-

tration. We have given necessary and sufficient analytic conditions for the existence of multiple steady states. Using estimated values of the parameters, we have numerically computed the range of the internal lactose concentration and growth rate for the existence of multiple steady states. From this, we conclude that the positive feedback loop involving permease is not necessary for the system to display bistability. Despite this conclusion, the permease regulatory pathway and other regulatory mechanisms (like inducer exclusion and catabolite repression) not considered in this study may play an important role in fine tuning the system bistable behavior and this must be addressed in future studies.

A local stability analysis of the model steady state shows that the steady states corresponding to both the lower and upper branches of the steady state A_* versus L curve are locally stable while the steady state on the middle branch is always unstable. Time delays due to transcription and translation have no effect on stability of the system in the sense that there is no evidence for a Hopf bifurcation although it was reported in a recent model developed for the regulation of *lac* operon by Mahaffy and Simeonov.¹⁶

The analysis of our reduced model gives no grounds to expect a Hopf bifurcation and the attendant oscillations that would ensue. The differences between the model of Mahaffy and Simeonov,¹⁶ where a Hopf bifurcation was found, and the current one are easily identified. In the Mahaffy and Simeonov model, the reaction between internal lactose and allolactose, which is catalyzed by β galactosidase, was ignored together with the individual degradation terms for the proteins. The latter leads to equal degradation rates because degradation is only due to the bacterial growth rate. Further, in Mahaffy and Simeonov¹⁶ they considered the lactose transport by permease into the cell as a fourth variable in the model. Consequently the local stability analysis of the model produced a characteristic equation similar to Eq. (C5), but in this case $P(\lambda)$ is a fourth order polynomial and $Q(\lambda)$ is a linear function of λ and this is the origin of the Hopf bifurcation. However, as in our results, Mahaffy and Simeonov¹⁶ concluded that the experimentally observed oscillations in the β galactosidase concentration reported by Knorre²⁹ were not caused by the induction process.

The accuracy of our model was tested against three different experimental data sets. The model is in reasonable agreement with the experimental data although the agreement is not perfect. The discrepancies between the experimental data and the simulations may originate from the differences in the experimental conditions and/or the simplifications in the model. One of the most interesting predictions of our model is the minimal intracellular lactose level for full induction of the system. The reduced model is also in good agreement with data reported in a recent study using an artificial inducer of the *lac* operon, Isopropylthiogalactoside (IPTG).³³ There it was found that 50–100 μM IPTG is sufficient as a lower bound to achieve full induction. Our reduced model predicts that the value should be 55.43 μM , which corresponds to the first “knee” in the A_* versus L curve in Fig. 4.

The analytical and numerical results obtained in this reduced model for the *lac* operon support and illuminate the

results reported in Yildirim and Mackey,²⁰ differing only in quantitative detail. For example, the full induction point in the reduced model was found to be 55.43 μM , whereas Yildirim and Mackey²⁰ found numerically that the induction point was 62.0 μM in the full model. Thus the reduced model seems to capture all of the essential properties of the full model investigated in Yildirim and Mackey.²⁰

Though the present reduced model is not accurate in all details, the results of the comparison with published and independent experimental data are sufficiently encouraging to prompt us to seek further sources of data for comparison, to find better estimates for the parameters, and to complete the analysis of the full model. One of the most robust predictions of the model is the existence of locally stable coexisting steady states depending on lactose levels and growth rate. This prediction is qualitatively confirmed by the observations of Novick and Wiener³⁴ and Cohn and Horibata,³⁵ and should be quantitatively testable.

The modeling carried out here, as in all of the other models cited earlier, is strictly deterministic in nature and based on the writing of chemical reaction equations. This approach is appropriate for the examination of the behavior of large numbers of the system in question, e.g., looking at the behavior of a large number of copies of the *lac* operon. It is worth noting, however, that if one were interested in the details of the dynamics at the level of a single bacterium a much different approach would have to be taken since the number of participating molecules may number in the tens to hundreds. In such a circumstance a stochastic modeling approach must be employed. Gillespie^{36,37} has considered in detail how *simulations* of such situations could be carried out, and variations of his scheme have been employed by a variety of authors to look at specific problems, e.g., Arkin *et al.*³⁸ examining phage- λ development, Morton-Firth and Bray³⁹ looking at dynamics of a flagellar motor, and Carrier and Keasling⁴⁰ investigating the *lac* operon. Other investigators are starting to put these simulation efforts on a firm theoretical footing, e.g., Paulsson *et al.*,⁴¹ Kepler and Elston⁴² and Swain *et al.*⁴³

ACKNOWLEDGMENTS

We thank Dr. Photini Pitsakis for her initial suggestion of this problem, and Professor Claire Cupples for her advice on parameter estimation and general comments. We also thank two anonymous referees for their comments and suggestions which measurably improved this paper. This work was supported by the Scientific and Technical Research Council of Turkey (TUBITAK), MITACS (Canada), the Natural Sciences and Engineering Research Council (NSERC Grant No. OGP-0036920, Canada), the Alexander von Humboldt Stiftung, Le Fonds pour la Formation de Chercheurs et l'Aide à la Recherche (FCAR Grant No. 98ER1057, Québec), the Leverhulme Trust (U.K.) and AIEJ Short-Term Exchange Promotion Program (Outbound) Scholarship (Japan).

APPENDIX A: PARAMETER ESTIMATION FOR THE REDUCED MODEL

In this appendix we detail how we have estimated the parameters in the reduced model described by Eqs. (7)–(9).

- μ : The maximal value of the dilution rate μ can be estimated from the shortest interdivision time of *E. coli* which is about 20 minutes.⁴⁴ Given this $\mu_{\max} = (\ln 2)/20 \text{ min}^{-1} = 3.47 \times 10^{-2} \text{ min}^{-1}$. We estimated a value for the growth rate $\bar{\mu}$ to be used in our numerical simulations together with the value of γ_A by least square fitting of the experimental β -galactosidase concentration data given in Knorre²⁹ using the FMINSEARCH and DDE23³⁰ routines in MATLAB. We found $\bar{\mu} \approx 3.03 \times 10^{-2} \text{ min}^{-1}$ indicating that these cultures were growing at close to their maximal rate. The results of estimation were tested for several initial starting points for μ and γ_A , and the estimation procedure always converged to the same values for both $\bar{\mu}$ and γ_A .
- γ_A : The value of γ_A was estimated as $1.35 \times 10^{-2} \text{ min}^{-1}$ together with the value of $\bar{\mu}$ by using least square fitting of the experimental β -galactosidase activity data given in Knorre²⁹ as above.
- γ_M : Leive and Kollin⁴⁵ found that the $t_{1/2}$ of β -galactosidase m-RNA was 2 minutes to give a value of $\gamma_M \approx \ln 2/2 = 0.347 \text{ min}^{-1}$. In a comparable experiment Blundell and Kennell⁴⁶ found $t_{1/2} = 1.47 \text{ min}$ to give $\gamma_M \approx 0.475 \text{ min}^{-1}$. We have taken the average of these two figures to give $\gamma_M \approx 0.411 \text{ min}^{-1}$.
- γ_B : The rate of breakdown of β -galactosidase was measured by Mandelstam⁴⁷ and found to be 5×10^{-2} per hour corresponding to $8.33 \times 10^{-4} \text{ min}^{-1}$. Rotman and Spiegelman⁴⁸ reported that the maximal rate of breakdown of β -galactoside is $5.0 \times 10^{-3} \text{ min}^{-1}$ and noted that it is possibly much smaller than this value. We have taken the Mandelstam value.
- K : Yagil and Yagil²² analyzed a number of previously published data sets, and from their calculations we find that the average value is $K \approx 7200$.
- n : Again from Yagil and Yagil²² we have that the average of the Hill coefficient is 2.09. We have taken $n = 2$.
- K_1 : The average dissociation constant of effector–repressor complex was determined to be $K_1 \approx 2.52 \times 10^{-2} (\mu\text{M})^{-2}$ from the results of Yagil and Yagil.²²
- α_M : The steady state value of *lac* mRNA in the absence of induction is thought to be one molecule per cell. This corresponds to a “concentration” of 2.08 nM if we take the *E. coli* volume to be 8×10^{-16} liter. When the cells are maximally induced, the *lac* mRNA level is raised a thousand times compared to this uninduced steady state value according to Savageau.⁴⁹ From Eq. (7) at a steady state,

$$0 = \bar{\gamma}_M M_* - \frac{\alpha_M}{K} \quad \text{when } A_* = 0, \quad (\text{A1})$$

$$0 = \bar{\gamma}_M 1000 M_* - \alpha_M \quad \text{when } A_* \rightarrow \infty. \quad (\text{A2})$$

From Eqs. (A1) and (A2), α_M is $9.97 \times 10^{-4} \text{ mM-min}^{-1}$.

- α_B : At a steady state, from Eq. (8) we have

$$\alpha_B = \frac{\bar{\gamma}_B B_*}{M_*} e^{\mu \tau_B}. \quad (\text{A3})$$

Kennell and Reizman⁵⁰ reported that steady state value of β -galactosidase is about 20 molecules per cell which means that $B_*/M_* = 20$. Using the value of γ_B reported by Mandelstam,⁴⁷ we estimate $\alpha_B \approx 1.66 \times 10^{-2} \text{ min}^{-1}$.

- α_A : Huber *et al.*⁵¹ studied the kinetics of β -galactosidase and found $V_{\max} = 32.6 \text{ U/mg}$ of β -galactosidase and $K_M = 0.00253 \text{ M}$ when lactose was the substrate while $V_{\max} = 49.6 \text{ U/mg}$ of β -galactosidase and $K_M = 0.00120 \text{ M}$ when allolactose is the substrate. [U is defined as μM of glucose or galactose produced per minute.] Given that the molecular weight of β -galactosidase is 540 000 Da and $1 \text{ Da} = 1.66 \times 10^{-21} \text{ mg}$, one mole of β -galactosidase is equivalent to $6.02 \times 10^{23} \times 5.4 \times 10^5 \times 1.66 \times 10^{-21} = 5.39 \times 10^8 \text{ mg}$ of β -galactosidase so 1 mg of β -galactosidase is equivalent to $1.85 \times 10^{-3} \mu\text{mol}$. Therefore,

$$\alpha_A \approx \frac{32.6 \mu\text{mol}}{1.85 \times 10^{-3} \mu\text{mol min}} = 1.76 \times 10^4 \text{ min}^{-1}.$$

- β_A : From the data of Huber *et al.*⁵¹ we have $\beta_A \approx 2.7 \times 10^4 \text{ min}^{-1}$, while Martínez-Bilbao *et al.*⁵² gives $\beta_A \approx 1.8 \times 10^4 \text{ min}^{-1}$. We have taken the average of $\beta_A \approx 2.15 \times 10^4 \text{ min}^{-1}$.
- K_L : The volume of one *E. coli* is approximately 8.0×10^{-16} liter and its mass is about 1.7×10^{-12} gram to yield a density of $2.1 \times 10^3 \text{ gm/liter}$. The parameter K_L in our model corresponds to the parameter $K_{m,Lac}/\rho$ in Wong *et al.*¹⁷ and the values and the units of these two parameters reported in this paper are $\rho = 3.0 \times 10^2$ grams of dry cell weight/liter and $K_{m,Lac} = 0.14 \text{ mM}$ which means that $K_{m,Lac}/\rho = (1.4 \times 10^{-4})/(3.0 \times 10^2) = 4.6 \times 10^{-7} \text{ mol/gr}$. To obtain an estimate for K_L in M, we can multiply this value by the density of the cell which gives $K_L \approx 0.97 \text{ mM}$, in agreement with the value of 1.4 mM estimated by Martínez-Bilbao *et al.*⁵² We will take the former value.
- K_A : This parameter in our model corresponds to $K_{m,Allo}/\rho$ in the Wong *et al.* model,¹⁷ and they took $K_{m,Allo} \approx 2.8 \text{ mM}$. Hence, $K_{m,Allo}/\rho = (2.8 \times 10^{-4})/(3.0 \times 10^2) = 9.3 \times 10^{-7} \text{ mol/gr}$. Using the same idea followed in the estimation of K_L , the value of K_A can be calculated as 1.95 mM .
- τ_M : In this model we are considering the transcription and translation of two genes, *lacZ* and *lacY*. Translation of *lacZ* starts shortly after transcription initiation, and for the translation of *lacY* to begin, *lacZ* must be completely transcribed. Knowing that *lacZ* has 1022 amino acids and that the DNA chain elongation rate is at least 490 nucleotides per second, which is equivalent to 9800 amino acids per minute, according to Bremmer and Dennis,⁵³ the time for *lacZ* to be completely transcribed is at most

$$\tau_M \approx \frac{1022}{9800} = 0.1 \text{ min}.$$

This gives an upper bound on τ_M .

- τ_B : *lacZ* is 1022 amino acids long and the mRNA elongation rate varies between 12 and 33 amino acids per second according to Monar *et al.*⁵⁴ and Kennell and

Reizman.⁵⁰ Talkad *et al.*⁵⁵ also reported the translation rate changes from 8 to 15 amino acids per second. If we take the mRNA elongation as 8 amino acids per second to estimate an upper bound value for τ_B , we obtain

$$\tau_B \approx \frac{1022}{8 \times 60} = 2.12 \text{ min.}$$

If the elongation rate is 33 amino acids per second then we have $\tau_B \approx 1022/(33 \times 60) = 0.51$ min. Sorensen *et al.*⁵⁶ estimated an average value for τ_B of 82 s experimentally which is 1.37 min. We have taken the upper bound as $\tau_B \approx 2.12$ min, and used $\tau_B = 2.0$ min.

APPENDIX B: CONDITIONS FOR EXISTENCE OF ONE, TWO, AND THREE STEADY STATES IN THE REDUCED MODEL

Equation (19) is equivalent to a fourth order polynomial in the allolactose concentration. After appropriate rearrangement, it can be written in the form

$$Y(a_*) = a_*^4 + \Omega_3 a_*^3 + \Omega_2 a_*^2 + \Omega_1 a_* + \Omega_0 = 0, \quad (\text{B1})$$

where the coefficients are given by

$$\Omega_3 = \kappa - \frac{\sigma_1}{\Theta}, \quad (\text{B2})$$

$$\Omega_2 = K e^{2\hat{\mu}\hat{\tau}_M} - \frac{h(l)\kappa}{\Theta}, \quad (\text{B3})$$

$$\Omega_1 = \kappa K e^{2\hat{\mu}\hat{\tau}_M} - \frac{\sigma_1 e^{2\hat{\mu}\hat{\tau}_M}}{\Theta}, \quad (\text{B4})$$

$$\Omega_0 = -\frac{h(l)\kappa e^{2\hat{\mu}\hat{\tau}_M}}{\Theta} < 0, \quad (\text{B5})$$

and

$$\sigma_1 = h(l) - \frac{\hat{\beta}_A}{\hat{\alpha}_A}. \quad (\text{B6})$$

$Y(a_*)$ approaches $+\infty$ as a_* goes to $\pm\infty$ and $Y(0) = \Omega_0 < 0$, so there are several possibilities for the roots of the quartic Eq. (B1). We can formalize these for biologically meaningful (non-negative steady states) as follows.

Theorem 1: *The lac operon model has at least one non-negative steady state.*

Proof: Since $\lim_{a_* \rightarrow \pm\infty} Y(a_*) = +\infty$ and $Y(0) = \Omega_0 < 0$, there exists an $a_* \in (0, \infty)$ such that $Y(a_*) = 0$.

Theorem 2: *(Two or three steady states, derivative from Ungar⁵⁷) Let $Y(a_*)$ be given by Eq. (B1) with real coefficients Ω_i , $i = 0, 1, 2, 3$, given by Eqs. (B2)–(B5). Define ξ_2 by*

$$\xi_2 = \Omega_1 - \Omega_0 \Omega_3 / \xi_1, \text{ where } \xi_1 = \Omega_2 - \Omega_1 / \Omega_3, \quad (\text{B7})$$

and set

$$\Delta = 12\Omega_0 + \Omega_2^2 - 3\Omega_1\Omega_3, \quad (\text{B8})$$

$$\Lambda = 27\Omega_0\Omega_3^2 - 9\Omega_1\Omega_2\Omega_3 + 2\Omega_2^3 - 72\Omega_0\Omega_2 + 27\Omega_1^2, \quad (\text{B9})$$

and

$$\Pi = 3\Omega_3^2 - 8\Omega_2 + 8\Re\left(\sqrt[3]{\frac{\Lambda + \sqrt{\Lambda^2 - 4\Delta^3}}{2}}\right). \quad (\text{B10})$$

If there are three sign changes in the sequence $(1, \Omega_3, \xi_1, \xi_2, \Omega_0)$, and

- (1) If $\Lambda^2 - 4\Delta^3 = 0$ and $\Pi \geq 0$ for all three cubic roots of Eq. (B10), then the lac operon model has two steady states.
- (2) If $\Lambda^2 - 4\Delta^3 < 0$ and $\Pi \geq 0$ for all three cubic roots of Eq. (B10), then the lac operon model has three steady states.

Proof: The proof of this theorem is a direct consequence of the application of the Routh–Hurwitz criteria and a result of Ungar.⁵⁷

APPENDIX C: LINEAR STABILITY OF THE STEADY STATES OF THE REDUCED MODEL

Let $x = m - m_*$, $y = b - b_*$ and $z = a - a_*$, respectively, denote the deviations of the dimensionless mRNA, β -galactosidase and allolactose levels from their steady state values. Linearizing Eqs. (10)–(12) in the neighborhood of a steady state we obtain the following linear system of delay equations:

$$\frac{dx}{d\hat{t}} = \hat{\alpha}_M f'(a_*) z_{\hat{\tau}_M} - \hat{\gamma}_M x, \quad (\text{C1})$$

$$\frac{dy}{d\hat{t}} = \tilde{\alpha}_B x_{\hat{\tau}_B} - \hat{\gamma}_B y, \quad (\text{C2})$$

and

$$\frac{dz}{d\hat{t}} = \tilde{\alpha}_A y - \tilde{\beta}_A z, \quad (\text{C3})$$

wherein we have set

$$\tilde{\alpha}_A = \hat{\alpha}_A h(l) - \hat{\beta}_A g(a_*),$$

$$\tilde{\beta}_A = \hat{\beta}_A b_* g'(a_*) + \hat{\gamma}_A,$$

and

$$\tilde{\alpha}_B = \hat{\alpha}_B e^{-\hat{\mu}\hat{\tau}_B}.$$

Note that in order to have a biologically meaningful steady state, it is necessary that

$$\tilde{\alpha}_A > 0 \quad (\text{C4})$$

must be satisfied because of Eq. (17).

Assuming that we have solutions to Eqs. (C1)–(C3) of the form $e^{\lambda \hat{t}}$ it is an easy exercise to show that the characteristic equation for the eigenvalues λ has the form

$$P(\lambda) + Q(\lambda) e^{-\lambda \hat{\tau}} = 0, \quad (\text{C5})$$

in which

$$P(\lambda) = \lambda^3 + \eta_2 \lambda^2 + \eta_1 \lambda + \eta_0, \quad (\text{C6})$$

$$Q(\lambda) = \vartheta, \quad (\text{C7})$$

where

$$\begin{aligned}
\eta_2 &= (\hat{\gamma}_M + \hat{\gamma}_B + \tilde{\beta}_A) > 0, \\
\eta_1 &= (\hat{\gamma}_M \hat{\gamma}_B + \tilde{\beta}_A \hat{\gamma}_B + \tilde{\beta}_A \hat{\gamma}_M) > 0, \\
\eta_0 &= \hat{\gamma}_M \hat{\gamma}_B \tilde{\beta}_A > 0, \\
\vartheta &= -\tilde{\alpha}_A \tilde{\alpha}_B \hat{\alpha}_M f'(a_*) < 0,
\end{aligned} \tag{C8}$$

and f and g are as given by Eqs. (13) and (15), respectively.

1. Stability when the delays are zero

The characteristic equation of our model reduces to a third order polynomial equation when both $\hat{\tau}_M=0$ and $\hat{\tau}_B=0$. When the delays are zero, from the Routh–Hurwitz criteria it is easy to show that a steady state will be locally stable if and only if the coefficients of Eq. (C5) satisfy the following conditions:

- (1) $\eta_2 > 0$,
- (2) $\eta_0 + \vartheta > 0$, and
- (3) $\eta_2 \eta_1 - \eta_0 - \vartheta > 0$.

Since the polynomials and the coefficients in the characteristic equation of the *lac* operon model given in Eqs. (C5)–(C8) satisfy Conditions 1 and 3 above, Condition 2 determines the local stability of a steady state a_*^i .

In this case with the delays all set to zero, one can obtain more global information about the stability of the steady states. Assume in Eqs. (10) and (11), respectively, that $\dot{m} = \dot{b} = 0$ so we can write an equation for the rate of change of allolactose in the form

$$\frac{da}{dt} = C(a) \left\{ f(a) - \Theta \frac{a}{h(l) - \frac{\hat{\beta}_A}{\hat{\alpha}_A} g(a)} \right\}, \tag{C9}$$

where

$$C(a) = \frac{\hat{\alpha}_B \hat{\alpha}_M \hat{\alpha}_A}{\hat{\gamma}_B \hat{\gamma}_M} \left[h(l) - \frac{\hat{\beta}_A}{\hat{\alpha}_A} g(a) \right] > 0 \text{ for } a \geq 0.$$

Remember that $f(a)$ is the function left hand side (LHS) plotted in Fig. 3, while

$$\Theta \frac{a}{h(l) - \frac{\hat{\beta}_A}{\hat{\alpha}_A} g(a)},$$

is the function right hand side (RHS).

Now notice from Eq. (C9) that when $a=0$ we have $\dot{a} > 0$ while for $a \rightarrow \infty$ we have $\dot{a} \rightarrow -\infty$. A simple argument (use Fig. 3 to see this) suffices to show that: (a) If there is a single steady state it is stable; (b) if there are two steady states then one will be half stable and the other will be stable; (c) if there are three steady states then the lower and upper steady states are stable and the intermediate steady state is unstable. Thus we have the following pattern for stability of the steady states in which “S” denotes stable, “US” means unstable, and “HS” stands for half stable:

- (1) $a_*^1 : S$,
- (2) $a_*^1, a_*^2 \equiv a_*^3 : S, HS$,
- (3) $a_*^1, a_*^2, a_*^3 : S, US, S$,
- (4) $a_*^1 \equiv a_*^2, a_*^3 : HS, S$,
- (5) $a_*^3 : S$.

A numerical determination of the stable and unstable regions of the lactose–allolactose concentration space when delays are both zero gives results qualitatively identical with those shown in Fig. 4. However, the induction point is changed from 55.43 μM when the delays are included to 52.10 μM when they are neglected.

2. Stability when the delays are not zero

When $\hat{\tau}_M \neq 0$ and $\hat{\tau}_B \neq 0$, the characteristic equation of the reduced model becomes a cubic quasi polynomial equation of the form Eq. (C5).

Theorem 3: (*Unstable Region*) The system whose characteristic equation given by Eq. (C5) has an unstable steady state in the domain defined by Eq. (C4) if

$$\eta_0 + \vartheta < 0 \tag{C10}$$

holds.

Proof: Since $P(\lambda)$ has the form

$$P(\lambda) = (\lambda + \hat{\gamma}_M)(\lambda + \hat{\gamma}_B)(\lambda + \tilde{\beta}_A), \tag{C11}$$

and all $\hat{\gamma}_M, \hat{\gamma}_B$, and $\tilde{\beta}_A$ are positive real numbers, then assuming inequality (C10) we have $P(0) + \vartheta = \eta_0 + \vartheta < 0$. Since $P(\lambda)$ increases without bound for $\lambda > 0$, there is some positive λ such that $P(\lambda) + \vartheta = 0$.

Theorem 4: (*Stable Region*) The system whose characteristic equation is given by Eq. (C5) is locally stable in the domain defined by Eq. (C4) if

$$\eta_0 + \vartheta > 0 \tag{C12}$$

holds.

Proof: Let $\lambda = u + iv$ be a root of the characteristic equation given by Eq. (C5). Then we have

$$\|P(u + iv)\|^2 = \|Q(u + iv)\|^2 e^{-2u\tau}. \tag{C13}$$

Assume that $u \geq 0$. $P(\lambda)$ has the form of Eq. (C11) so $\eta_0^2 \leq \|P(u + iv)\|^2$. Since $\tau > 0$, $\|Q(u + iv)\|^2 e^{-2u\tau} = \vartheta^2 e^{-2u\tau} < \vartheta^2$ and it, therefore, follows that $\eta_0^2 - \vartheta^2 < 0$. However,

$$\eta_0^2 - \vartheta^2 = (\eta_0 - \vartheta)(\eta_0 + \vartheta). \tag{C14}$$

From Eq. (C8), we have $\eta_0 - \vartheta \geq 0$, so if $\eta_0 + \vartheta \geq 0$ then $\eta_0^2 - \vartheta^2 \geq 0$ and we have a contradiction. Hence, $u < 0$ and the system is stable for $\tau > 0$ and $\eta_0 + \vartheta > 0$.

The results of Theorems 3 and 4 allow us to assert that the stability results we found in the previous section with the delays equal to zero are maintained in the general case when they assume their positive values as detailed in Table I. This type of stability is very similar to the concept of *absolute stability* introduced by Brauer.⁵⁸ In Fig. 4 we show the numerically determined stable and unstable regions for the reduced *lac* operon model and a graph of the steady state

curve as a function of the external lactose concentration when all parameters are as in Table I and $\bar{\mu} = 3.03 \times 10^{-2} \text{ min}^{-1}$.

APPENDIX D: NATURE OF THE SLOPE OF THE STEADY STATE CURVE AT THE INTERSECTION POINT WITH THE STABILITY BOUNDARY CURVE

To prove that the separating point between the middle and lower (upper) branch is located exactly on the boundary between stable and unstable regions, it is enough to show that the derivative da_*/dl of the steady state curve is equal to $\pm\infty$ at the intersection point(s) of the boundary curve and the steady state (hysteresis) curve. This is equivalent to $dl/da_* = 0$.

From the steady state equation given by Eq. (19), we have

$$\tilde{\alpha}_A f(a_*) - \Theta \hat{\alpha}_A a_* = 0. \quad (\text{D1})$$

The boundary curve between stable and unstable regions, which is given by Eq. (C10), can also be written as

$$\hat{\gamma}_M \hat{\gamma}_B \tilde{\beta}_A - \tilde{\alpha}_A \tilde{\alpha}_B \hat{\alpha}_M f'(a_*) = 0. \quad (\text{D2})$$

Substituting $\tilde{\beta}_A$ and Eq. (17) into Eq. (D2), we have

$$\hat{\gamma}_A \hat{\gamma}_B \hat{\gamma}_M \left(\frac{\hat{\beta}_A a_* g'(a_*)}{\tilde{\alpha}_A} + 1 \right) - \tilde{\alpha}_A \hat{\alpha}_A \hat{\alpha}_B \hat{\alpha}_M e^{-\hat{\mu} \hat{\tau}_B} \frac{f'(a_*)}{\hat{\alpha}_A} = 0. \quad (\text{D3})$$

Taking the factor $\tilde{\alpha}_A \hat{\alpha}_A \hat{\alpha}_B \hat{\alpha}_M e^{-\hat{\mu} \hat{\tau}_B}$ outside of the parenthesis, we obtain

$$\frac{\hat{\gamma}_A \hat{\gamma}_B \hat{\gamma}_M}{\hat{\alpha}_A \hat{\alpha}_B \hat{\alpha}_M e^{-\hat{\mu} \hat{\tau}_B}} \left(\frac{\hat{\beta}_A a_* g'(a_*)}{\tilde{\alpha}_A} + 1 \right) - \tilde{\alpha}_A \frac{f'(a_*)}{\hat{\alpha}_A} = 0. \quad (\text{D4})$$

Writing Θ instead of the expression given by Eq. (20) we can rewrite this last expression as

$$\Theta \hat{\alpha}_A \left(\frac{\hat{\beta}_A a_* g'(a_*)}{\tilde{\alpha}_A} + 1 \right) - \tilde{\alpha}_A f'(a_*) = 0. \quad (\text{D5})$$

Finally, we obtain

$$f'(a_*) \tilde{\alpha}_A - \hat{\alpha}_A \Theta - \frac{\hat{\alpha}_A \Theta \hat{\beta}_A a_* g'(a_*)}{\tilde{\alpha}_A} = 0. \quad (\text{D6})$$

By computing the derivative dl/da_* from Eq. (D1), we have

$$f(a_*) \left(\hat{\alpha}_A \frac{\sqrt{K_1} K_L}{(\sqrt{K_1} K_L + l)^2} - \hat{\beta}_A g'(a_*) \frac{da_*}{dl} \right) + \tilde{\alpha}_A f'(a_*) \frac{da_*}{dl} - \hat{\alpha}_A \Theta \frac{da_*}{dl} = 0, \quad (\text{D7})$$

and writing dl/da_* explicitly,

$$\frac{dl}{da_*} = - \frac{\tilde{\alpha}_A f'(a_*) - \hat{\beta}_A g'(a_*) f(a_*) - \hat{\alpha}_A \Theta}{\hat{\alpha}_A f(a_*) \frac{\sqrt{K_1} K_L}{(\sqrt{K_1} K_L + l)^2}} \quad (\text{D8})$$

results. The denominator in Eq. (D8) is always nonzero.

Turning back to Eq. (D1), we can write

$$\tilde{\alpha}_A = \frac{\Theta \hat{\alpha}_A a_*}{f(a_*)}, \quad (\text{D9})$$

and substituting Eq. (D9) into the equation obtained from the boundary curve given by Eq. (D6), we have

$$\tilde{\alpha}_A f'(a_*) - \hat{\beta}_A g'(a_*) f(a_*) - \hat{\alpha}_A \Theta = 0. \quad (\text{D10})$$

Substituting this expression into Eq. (D6) completes the proof. Thus, the tangents drawn to the steady state curve at the intersection points with the stability curve have infinite slope.

APPENDIX E: A BIFURCATION DEPENDENT ON LACTOSE LEVELS AND GROWTH RATE

To estimate the critical value for bacterial growth rate at which the *lac* operon model switches from a single steady state to multiple steady states, we used the following technique. Changing the bacterial growth rate from 0 to μ_{\max} with a certain step size $\Delta\mu$, we determined an interval for μ giving a range for the lactose concentration for existence of three steady states using Theorem B. Then dividing this interval into subintervals, we repeated the same procedure and estimated an interval for μ in which the critical value μ_0 takes place.

Consider the cases of $\mu = \mu_{\max} = 3.47 \times 10^{-2} \text{ min}^{-1}$ and $\mu = 0 \text{ min}^{-1}$. Since $L > 0$, for all $\mu \in (0, 3.47 \times 10^{-2}) \text{ min}^{-1}$ when all the other parameters are held constant at their estimated values given in Table I, we have

$$\begin{aligned} \Omega_0 &< 0, \\ \Omega_3 &> 0, \\ 3\Omega_3^2 - 8\Omega_2 &> 0. \end{aligned}$$

The *lac* operon model has three steady states if the conditions

$$\begin{aligned} \xi_1 &< 0, \\ \xi_2 &> 0, \\ \Lambda^2 - 4\Delta^3 &< 0, \\ \Pi &\geq 0, \end{aligned}$$

are all satisfied simultaneously.

When $\mu = 3.47 \times 10^{-2} \text{ min}^{-1}$, we can calculate the first three of these conditions as

$$\begin{aligned} \xi_1 &< 0 \Leftrightarrow L > 0.40031 \text{ } \mu\text{M}, \\ \xi_2 &> 0 \Leftrightarrow 0 < L < 0.40031 \text{ } \mu\text{M} \\ &\text{or } L > 0.41277 \text{ } \mu\text{M}, \end{aligned}$$

$$\Lambda^2 - 4\Delta^3 < 0 \Leftrightarrow 44.63609 \text{ } \mu\text{M} < L < 70.78300 \text{ } \mu\text{M}.$$

Since

$$\Pi > 3\Omega_3^2 - 8\Omega_2 - 8\sqrt{\Delta} \equiv \Pi',$$

we have

$$\Pi > \Pi' > 0$$

for L in (44.636 09, 70.783 00) μM . Hence, the relationship between L and A_* shows hysteresis when $\mu = 3.47 \times 10^{-2} \text{ min}^{-1}$, and there exist three steady states when L is between 44.636 09 and 70.783 00 μM . On the other hand, when $\mu = 0 \text{ min}^{-1}$,

$$\xi_1 < 0 \Leftrightarrow L > 2.254 77 \text{ nM},$$

$$\xi_2 > 0 \Leftrightarrow 0 < L < 2.254 77 \text{ nM} \text{ or } L > 14.620 79 \text{ nM},$$

but for all $L > 0$,

$$\Lambda^2 - 4\Delta^3 > 0.$$

Therefore, the relationship between L and A_* does not show hysteresis when $\mu = 0 \text{ min}^{-1}$.

We found that the critical value of μ_0 for the existence of multiple steady states was $\mu_0 \in (1.51 \times 10^{-2}, 1.52 \times 10^{-2}) \text{ min}^{-1}$, and thus for all values of $\mu \in (\mu_0, \mu_{\max})$ bistable behavior is predicted.

- ¹J. Beckwith, "The operon: An historical account" in *Escherichia coli and Salmonella: Cellular and Molecular Biology*, edited by F. C. Neidhardt (American Society for Microbiology, Washington, D.C., 1987), Vol. 2, pp. 1439–1443.
- ²F. Jacob, D. Perrin, C. Sanchez, and J. Monod, "L'Operon: groupe de gène à expression par un operateur," *C. R. Seances Acad. Sci. III* **250**, 1727–1729 (1960).
- ³A. Novick and M. Wiener, "Enzyme induction as an all-or-none phenomenon," *Proc. Natl. Acad. Sci. U.S.A.* **43**, 553–566 (1957).
- ⁴M. Laurent and N. Kellershohn, "Multistability: A major means of differentiation and evolution in biological systems," *Trends Biochem. Sci.* **24**, 418–422 (1999).
- ⁵J. Casadesús and R. D'Ari, "Memory in bacteria and phage," *BioEssays* **24**, 512–518 (2002).
- ⁶J. E. Ferrel, Jr., "Self-perpetuating states in signal transduction: Positive feedback, double-negative feedback, and bistability," *Curr. Opin. Cell Biol.* **14** (2), 140–148 (2002).
- ⁷J. S. Griffith, "Mathematics of cellular control processes. II. Positive feedback to one gene," *J. Theor. Biol.* **20**, 209–216 (1968).
- ⁸A. Babloyantz and M. Sanglier, "Chemical instabilities of all or none type in β -galactosidase induction and active transport," *FEBS Lett.* **23**, 364–366 (1972).
- ⁹M. Sanglier and G. Nicolis, "Sustained oscillations and threshold phenomena in an operon control circuit," *Biophys. Chem.* **4**, 113–121 (1976).
- ¹⁰J. J. Tyson and H. G. Othmer, "The dynamics of feedback control circuits in biochemical pathways," in *Progress in Biophysics*, edited by R. Rosen (Academic, New York, 1978), Vol. 5, pp. 1–62.
- ¹¹J. F. Selgrade, "Mathematical analysis of a cellular control process with positive feedback," *SIAM (Soc. Ind. Appl. Math.) J. Appl. Math.* **36**, 219–229 (1979).
- ¹²J. F. Selgrade, "A Hopf bifurcation in single loop positive feedback systems," *Q. Appl. Math.* **40**, 347–351 (1982).
- ¹³J. Ji-Fa, "A Liapunov function for four dimensional positive feedback systems," *Q. Appl. Math.* **52**, 601–614 (1994).
- ¹⁴J. M. Mahaffy, "Cellular control models with linked positive and negative feedback and delays. I. The models," *J. Theor. Biol.* **106**, 89–102 (1984).
- ¹⁵J. M. Mahaffy, "Cellular control models with linked positive and negative feedback and delays. II. Linear analysis and local stability," *J. Theor. Biol.* **106**, 103–118 (1984).
- ¹⁶J. M. Mahaffy and E. Simeonov, "Stability analysis for a mathematical model of the *lac* operon," *Q. Appl. Math.* **57**, 37–53 (1999).
- ¹⁷P. Wong, S. Gladney, and J. D. Keasling, "Mathematical model of the *lac* operon: Inducer exclusion, catabolite repression, and diauxic growth on glucose and lactose," *Biotechnol. Prog.* **13**, 132–143 (1997).
- ¹⁸B. Cheng, R. L. Fournier, and P. A. Relue, "The inhibition of *Escherichia coli lac* operon gene expression by antigene oligonucleotides—Mathematical modeling," *Biotechnol. Bioeng.* **70**, 467–472 (2000).
- ¹⁹B. Cheng, R. L. Fournier, P. A. Relue, and J. Schisler, "An experimental and theoretical study of the inhibition of *Escherichia coli lac* operon gene expression by antigene oligonucleotides," *Biotechnol. Bioeng.* **74**, 220–229 (2001).
- ²⁰N. Yildirim and M. C. Mackey, "Feedback regulation in the lactose operon: A mathematical modeling study and comparison with experimental data," *Biophys. J.* **84**, 2841–2851 (2003).
- ²¹J. Beckwith, "The lactose operon," in *Escherichia coli and Salmonella: Cellular and Molecular Biology*, edited by F. C. Neidhardt (American Society for Microbiology, Washington, D.C., 1987), Vol. 2, pp. 1444–1452.
- ²²G. Yagil and E. Yagil, "On the relation between effector concentration and the rate of induced enzyme synthesis," *Biophys. J.* **11**, 11–27 (1971).
- ²³These dilution terms can be understood as follows. Consider a species x that is being degraded at a rate μ , so $dx/dt = -\mu x$. This explains the nature of the linear degradation terms. Then if we integrate this equation from $t - \tau$ [concentration $x(t - \tau)$] to t [concentration $x(t)$] we obtain $x(t) = x(t - \tau) \exp(-\mu\tau)$ which explains the nature of the exponential dilution factors $\exp(-\mu\tau)$ related to concentrations evaluated at a time $t - \tau$.
- ²⁴M. H. Saier, "Inducer exclusion and regulation of the melibiose, maltose, glycerol, and lactose transport systems by the phosphoenolpyruvate: Sugar phosphotransferase system," *J. Biol. Chem.* **251**, 6606–6615 (1976).
- ²⁵T. Osumi and M. H. Saier, "Regulation of lactose permease activity by the phosphoenolpyruvate:sugar phosphotransferase system: Evidence for direct binding of the glucose specific enzyme III to the lactose permease," *Proc. Natl. Acad. Sci. U.S.A.* **79**, 1457–1461 (1982).
- ²⁶P. W. Postma, J. W. Lengeler, and G. R. Jacobson, "Phosphoenolpyruvate-carbohydrate phosphotransferase systems," in *Escherichia coli and Salmonella: Cellular and Molecular Biology*, edited by F. C. Neidhardt (American Society for Microbiology, Washington, D.C., 1996), Vol. 1, pp. 1149–1174.
- ²⁷M. H. Saier, T. M. Ramseier, and J. Reizer, "Regulation of carbon utilization," in *Escherichia coli and Salmonella: Cellular and Molecular Biology*, edited by F. C. Neidhardt (American Society for Microbiology, Washington, D.C., 1996), Vol. 1, pp. 1325–1343.
- ²⁸We have been unable to find experimental verification of this assumption, though preliminary parameter estimations in the full model and those by Wong *et al.* (Ref. 17) support our assumption. This assumption concerning the rapid equilibration of intra- and extra-cellular lactose can, and should, be checked experimentally.
- ²⁹W. A. Knorre, "Oscillation of the rate of β galactosidase in *Escherichia coli* ML 30 and ML 308," *Biochem. Biophys. Res. Commun.* **31** (5), 812–817 (1968).
- ³⁰L. F. Shampine and S. Thompson, "Solving DDEs with MATLAB," www.radford.edu/~thompson/webdides/ (2000).
- ³¹S. Pestka, B. L. Daugherty, V. Jung, K. Hotta, and R. K. Pestka, "AntimRNA: specific inhibition of translation of single mRNA molecules," *Proc. Natl. Acad. Sci. U.S.A.* **81**, 7525–7528 (1984).
- ³²B. C. Goodwin, "Control dynamics of β galactosidase in relation to the bacterial cell cycle," *Eur. J. Biochem.* **10** (3), 515–522 (1969).
- ³³F. Baneyx, "Recombinant protein expression in *Escherichia coli*," *Curr. Opin. Biotechnol.* **10**(5), 411–421 (1999).
- ³⁴A. Novick and M. Wiener, "Induction as an all-or-none phenomenon," *Proc. Natl. Acad. Sci. U.S.A.* **43**, 553–566 (1957).
- ³⁵M. Cohn and K. Horibata, "Inhibition by glucose of the induced synthesis of the β -galactosidase-enzyme system of *Escherichia coli*: Analysis of maintenance," *J. Bacteriol.* **78**, 613–623 (1959).
- ³⁶D. T. Gillespie, "Exact stochastic simulation of coupled chemical reactions," *J. Phys. Chem.* **81**, 2340–2361 (1977).
- ³⁷D. T. Gillespie, "A rigorous derivation of the chemical master equation," *Physica A* **188**, 404–425 (1992).
- ³⁸A. Arkin, J. Ross, and H. H. McAdams, "Stochastic kinetic analysis of developmental pathway bifurcation in phage λ -infected *Escherichia coli* cells," *Genetics* **149** (4), 1633–48 (1998).
- ³⁹C. J. Morton-Firth and D. Bray, "Predicting temporal fluctuations in an intracellular signaling pathway," *J. Theor. Biol.* **192**, 117–128 (1998).
- ⁴⁰T. A. Carrier and J. D. Keasling, "Investigating autocatalytic gene expression systems through mechanistic modeling," *J. Theor. Biol.* **201**, 25–36 (1999).
- ⁴¹J. Paulsson, O. G. Berg, and M. Ehrenberg, "Stochastic focusing: Fluctuation-enhanced sensitivity of intracellular regulation," *Proc. Natl. Acad. Sci. U.S.A.* **97**, 7148–7153 (2000).
- ⁴²T. B. Kepler and T. C. Elston, "Stochasticity in transcriptional regulation: Origins, consequences, and mathematical representations," *Biophys. J.* **81**, 3116–3136 (2001).

- ⁴³P. S. Swain, M. B. Elowitz, and E. D. Siggia, "Intrinsic and extrinsic contributions to stochasticity in gene expression," *Proc. Natl. Acad. Sci. U.S.A.* **99**, 12795–12800 (2002).
- ⁴⁴J. D. Watson, *Molecular Biology of the Gene* (Benjamin, New York, 1977).
- ⁴⁵L. Leive and V. Kollin, "Synthesis, utilization and degradation of lactose operon mRNA in *Escherichia coli*," *J. Mol. Biol.* **24**, 247–259 (1967).
- ⁴⁶M. Blundell and D. Kennell, "Evidence for endonucleolytic attack in decay of *lac* messenger RNA in *Escherichia coli*," *J. Mol. Biol.* **83**, 143–161 (1974).
- ⁴⁷J. Mandelstam, "Turnover of protein in starved bacteria and its relationship to the induced synthesis of enzyme," *Nature (London)* **4571**, 1179–1181 (1957).
- ⁴⁸R. Rotman and S. Spiegelman, "On the origin of the carbon in induced synthesis of β -galactosidase," *J. Bacteriol.* **68**, 419–429 (1954).
- ⁴⁹M. A. Savageau, "Design of gene circuitry by natural selection: Analysis of the lactose catabolic system in *Escherichia coli*," *Biochem. Soc. Trans.* **27** (2), 264–270 (1999).
- ⁵⁰D. Kennell and H. Reizman, "Transcription and translation initiation frequencies of the *Escherichia coli lac* operon," *J. Mol. Biol.* **114**, 1–21 (1977).
- ⁵¹R. E. Huber, W. Wallenfels, and G. Kurz, "The action of β -galactosidase *Escherichia coli* on allolactose," *Can. J. Biochem.* **53**, 1035–1039 (1975).
- ⁵²M. Martínez-Bilbao, R. E. Holdswards, L. A. Edwards, and R. E. Hube, "A highly reactive beta galactosidase *Escherichia coli* resulting from a substitution of an aspartic acid for Gly-794," *J. Biol. Chem.* **266** (8), 4979–4986 (1991).
- ⁵³H. Bremmer and P. P. Dennis, "Modulation of chemical composition and other parameters of the cell by growth rate," in *Escherichia coli and Salmonella: Cellular and Molecular Biology*, edited by F. C. Neidhardt (American Society for Microbiology, Washington, D.C., 1996), Vol. 2, pp. 1553–1569.
- ⁵⁴H. Monar, D. Goodman, and G. S. Stnet, "RNA chain growth rates in *Escherichia coli*," *J. Mol. Biol.* **39**, 1–29 (1969).
- ⁵⁵V. Talkad, E. Schneider, and D. Kennell, "Evidence for variable rates of ribosome movement in *Escherichia coli*," *J. Mol. Biol.* **104** (1), 299–303 (1976).
- ⁵⁶M. A. Sorensen, C. G. Kurland, and S. Pedersen, "Codon usage determines translation rate in *Escherichia coli*," *J. Mol. Biol.* **207** (2), 365–77 (1989).
- ⁵⁷A. A. Ungar, "An unified approach for solving quadratic, cubic and quartic equations by radicals," *Comput. Math. Appl.* **19** (12), 33–39 (1990).
- ⁵⁸F. Brauer, "Absolute stability in delay equations," *J. Diff. Eqns.* **69**, 185–191 (1987).